HHS Public Access

Author manuscript

Adv Funct Mater. Author manuscript; available in PMC 2017 August 23.

Published in final edited form as:

Adv Funct Mater. 2016 August 23; 26(32): 5873–5883. doi:10.1002/adfm.201601146.

Multi-Material Tissue Engineering Scaffold with Hierarchical Pore Architecture

Dr. Kathy Ye Morgan,
Harvard-MIT Division of Health Sciences and Technology, David H. Koch Institute for Integrative Cancer Research, and Institute for Medical Engineering & Science, Massachusetts Institute of Technology, Cambridge, MA 02139, USA

Demetra Sklaviadis,
Harvard-MIT Division of Health Sciences and Technology, David H. Koch Institute for Integrative Cancer Research, and Institute for Medical Engineering & Science, Massachusetts Institute of Technology, Cambridge, MA 02139, USA

Zachary L. Tochka,
Harvard-MIT Division of Health Sciences and Technology, David H. Koch Institute for Integrative Cancer Research, and Institute for Medical Engineering & Science, Massachusetts Institute of Technology, Cambridge, MA 02139, USA

Dr. Kristin M. Fischer,
Harvard-MIT Division of Health Sciences and Technology, David H. Koch Institute for Integrative Cancer Research, and Institute for Medical Engineering & Science, Massachusetts Institute of Technology, Cambridge, MA 02139, USA

Dr. Keith Hearon,
Harvard-MIT Division of Health Sciences and Technology, David H. Koch Institute for Integrative Cancer Research, and Institute for Medical Engineering & Science, Massachusetts Institute of Technology, Cambridge, MA 02139, USA

Thomas D. Morgan,
Harvard University School of Engineering & Applied Science, Cambridge, MA 02138, USA

Dr. Robert Langer, and
Harvard-MIT Division of Health Sciences and Technology, David H. Koch Institute for Integrative Cancer Research, and Institute for Medical Engineering & Science, Massachusetts Institute of Technology, Cambridge, MA 02139, USA

Dr. Lisa E. Freed
Harvard-MIT Division of Health Sciences and Technology, David H. Koch Institute for Integrative Cancer Research, and Institute for Medical Engineering & Science, Massachusetts Institute of Technology, Cambridge, MA 02139, USA. Materials Engineering Division, Draper, Cambridge, MA 02139, USA

Lisa E. Freed: lfreed@draper.com, lfreed@mit.edu

Correspondence to: Lisa E. Freed, `lfreed@draper.comlfreed@mit.edu`.

Abstract

Multi-material polymer scaffolds with multiscale pore architectures were characterized and tested with vascular and heart cells as part of a platform for replacing damaged heart muscle. Vascular and muscle scaffolds were constructed from a new material, poly(limonene thioether) (PLT32i), which met the design criteria of slow biodegradability, elastomeric mechanical properties, and facile processing. The vascular-parenchymal interface was a poly(glycerol sebacate) (PGS) porous membrane that met different criteria of rapid biodegradability, high oxygen permeance, and high porosity. A hierarchical architecture of primary (macroscale) and secondary (microscale) pores was created by casting the PLT32i prepolymer onto sintered spheres of poly(methyl methacrylate) (PMMA) within precisely patterned molds followed by photocuring, de-molding, and leaching out the PMMA. Pre-fabricated polymer templates were cellularized, assembled, and perfused in order to engineer spatially organized, contractile heart tissue. Structural and functional analyses showed that the primary pores guided heart cell alignment and enabled robust perfusion while the secondary pores increased heart cell retention and reduced polymer volume fraction.

Graphical abstract

A biodegradable elastomeric polymer template with slowly and rapidly degrading components and a hierarchical architecture of primary (macroscale) and secondary (microscale) pores enables heart and vascular cells to form organized engineered cardiac tissue. The platform supports microvessel perfusion and contractile heart muscle formation in vitro and, if validated in vivo, may aid in the regenerative repair of vascularized tissues.

Keywords

polymer; heart cell; endothelial cell; microfluidic; multiscale

1. Introduction

Heart muscle is a highly organized tissue with high metabolic demand and consequently the disruption of its life-sustaining blood vessels causes high morbidity and mortality.[1] Recent progress suggests that cell therapy has the potential to revolutionize the treatment of infarcted myocardium by enabling revascularization and restoring physiological contractile function,[2] and creating perfusable capillaries.[3] However, maintaining survival and function at the cellular level is particularly challenging during scale-up from micro-tissue to thicker heart muscle.[4] Nearly all tissues have evolved a complex internal vasculature that provides convective-diffusive transport to the parenchymal (i.e., tissue-specific) cells. Many parenchymal cells, including cardiomyocytes, must reside within a few hundred μm of perfusable conduits with permeable interfaces because these cells require efficient oxygen (O_2) transport to remain alive.[5]

Emerging material technologies offer unprecedented opportunities for engineering complex three dimensional (3D) tissues.[6] Scaffolds and cellularized tissue-like constructs with discrete compartments for cardiomyocytes and vascular cells have been created by 3D printing of hydrogel and extracellular matrix-based inks, cell-laden bioinks, sacrificial

lattices and fugitive inks that can be transformed into microchannels,[7] and cellularization of pre-fabricated polymer templates.[4b, 8] For soft tissue engineering applications, tough, biodegradable elastomers,[9] such as PGS,[10] have been invented based on the reasoning that materials to be implanted into mechanically dynamic environments will function more optimally if constructed from compliant materials that can recover from large deformation and then dissolve in the body at a rate matching that of tissue repair. As compared with naturally derived scaffolds,[11] notable advantages of using synthetic polymer scaffolds are their well-defined and highly tunable chemical and mechanical properties, and finer control over degradation kinetics.[9, 12]

Our tissue engineering approach relies on mechanically robust polymer scaffolds that can support the cardiac cycle (i.e., systole, diastole), provide perfusable flow conduits, and biodegrade by surface erosion.[4a] Previous studies of polymer grids with patterned through-pores have demonstrated (i) contractile engineered cardiac muscle,[13] (ii) elastomeric mechanical properties mimicking native heart muscle (i.e., compliance, high strain-to-failure, and anisotropy),[13a, 14] (iii) myocyte alignment,[13a–c, 15] and (iv) prolonged retention of exogenous heart cells in a subcutaneous implantation model.[16] Related studies of polymers with patterned microfluidics have demonstrated (i) perfusion-mediated increase in the viability of myocytes cultured in an adjacent parenchymal compartment,[8b, 17] and (ii) host-mediated angiogenesis upon implantation.[17] However, previous polymer-based cardiac grafts did not meet the key physiological requirement of scalable transport between heart cells and endothelialized microchannels.

In the present study, pre-fabricated polymer templates were cellularized, assembled, and perfused to create pre-vascularized, contractile engineered cardiac tissue. Introduction of micropores throughout a precisely patterned 3D macroporous framework that was designed to provide perfusion and mechanical anisotropy distinguishes our approach from other multi-compartmental scaffolds.[4b, 8a, 11a] Also, muscle and vascular templates were constructed from a novel slowly degrading elastomer, PLT32i, and were connected via an oxygen permeable vascular-parenchymal interface constructed from rapidly biodegrading PGS.

2. Results and Discussion

2.1. Material Formulation, Processing, and Characterization

PLT32i was intentionally designed to exhibit certain material advantages of our recently reported photocurable thiol-ene elastomer, PLT32o, which included facile synthesis and processing and long term in vivo retention of 3D structural integrity and heart cells,[16] while also exhibiting a biodegradation rate slower than that of PGS (Figure 1A). PLT32i and PLT32o were network polymers comprised of an alkene macromonomer and a difunctional thiol co-monomer. The macromonomer was trimethylolpropane tris(3-mercaptopropionate) (TMPTMP) end-capped with D-limonene, and the co-monomer was either tetraethylene glycol bis(2-mercaptopropionate) (TEGBMP) for PLT32i or 1,10 decanedithiol (1,10 DDT) for PLT32o. PGS was the branched polymerization product of glycerol and sebacic acid.[10a] PLT32i and PLT32o prepolymers were synthesized by solvent-free one-pot photoreactions, and both were curable upon exposure to 365 nm UV light under ambient conditions,

whereas PGS synthesis required a nitrogen (N_2) atmosphere and curing under extreme conditions of heat and vacuum for extended time periods.[9b, 10a, 16, 18]

In vitro biodegradation studies were performed on PLT32o, PLT32i, and PGS blocks that were rendered porous using a commercially available template of sintered 30 ± 2 μm acrylic spheres.[19] Porous polymer blocks were incubated at 37°C in either enzyme (lipase) or phosphate buffered saline, and dry mass loss was quantified (Figure 1B). PLT32o did not degrade under either condition tested, PLT32i did not degrade in buffered saline and degraded slowly in a linear fashion in lipase, while PGS degraded rapidly in a linear fashion both in buffer for 16 weeks and in lipase over the first 4 weeks. The finding that PLT32i degraded slowly and in a linear manner in lipase is consistent with a mechanism of surface erosion by an enzyme that is capable of hydrolyzing ester bonds. The PGS degradation data are consistent with a seminal study that introduced the material and established degradation by hydrolytic cleavage in buffer,[10a] and a subsequent study showing solid PGS membrane thickness decreased in a linear manner during short term (12 h) incubation in lipase.[18] During the present study, which involved porous specimens and a substantially longer (16 week) lipase incubation, PGS mass loss tapered off after 4 weeks which we speculate may be attributable to the porous nature of the specimen and/or increasingly restricted diffusional transport over time.[20] The finding of more rapid degradation for PLT32i than PLT32o can be attributed to relatively higher hydrophilicity of the respective co-monomers (i.e., higher for TEGBMP than 1,10 DDT). The finding of of more rapid degradation for PGS than PLT32i can be attributed to higher average ester composition per network repeat unit and higher hydrophilicity of component monomers for PGS than PLT32i.

Oxygen transport is critical for cell survival, and the slow transport of dissolved O_2 through most materials is a factor limiting the utility of polymer scaffolds for tissue engineering.[2c, 4a, 5c, 21] Moreover, reducing the polymer volume fraction of a tissue engineering scaffold can, in principle, reduce physical barriers to cellularization and implant integration.[2c, 5c, 21] In an effort to accelerate O_2 transport and reduce polymer volume fraction for PLT32i, PLT32o and PGS materials, microscale pores were introduced using sintered PMMA microspheres (5 to 38 μm) by adapting an established technique shown to afford well-defined, easily tunable, functional pore geometries,[4b, 19] that was recently demonstrated for PGS.[8b]

A Franz diffusion cell fitted with fiber-optic sensors was used to measure the O_2 permeance of solid or porous PLT32i, PLT32o and PGS membranes according to Equation(1) as previously described:[22]

$$Permeance \frac{cm^3(S.T.P.)}{cm^2 s\, cmHg} = -ln\left(\frac{P_1 - P_2}{P_1}\right)\frac{V\, S_w}{A\, t} \quad (1)$$

where P_1 and P_2 are respectively the partial pressures of O_2 in water in the donor (high-O_2) and acceptor (low-O_2) chambers of the Franz cell, V is the volume of water in the Franz cell (2 cm^3), A is the surface area of the membrane (1.8 cm^2) and S_w is the solubility of O_2 in

water at 25°C (2.83×10^{-2} cm^3(S.T.P.) cm^{-3} atm^{-1}).[23] The porosities of PLT32i, PLT32o and PGS membranes were calculated using Equation (2):[24]

$$Porosity = 1 - \frac{\rho_{porous\ material}}{\rho_{solid\ material}} \quad (2)$$

where the densities (ρ) of the solid and porous materials were obtained by measuring diameter, thickness, and dry mass of die-punched disks.[18]

The presence of secondary micropores significantly increased O_2 permeance (Figure 1C) and reduced polymer volume fraction by introducing porosities in the range of 54 to 72% (Figure 1D). The finding that permeance and porosity were significantly higher for porous membranes made of PGS as compared with those made of PLT32i may be explained by differences between bulk material network structures (a branched polymer structure for PGS *versus* a network polymer for PLT32i) and/or by the generation of microscale pores in the PGS during curing by thermal crosslinking.[24a] Structural analyses of microscale pore size variations can be quantified in a future study.

2.2. Multi-material Scaffolds with Hierarchical Pore Architectures

To explore the influence of scaffold design on cell retention, alignment, and function, multi-material polymer scaffolds with hierarchical pore architectures were developed for culturing vascular and heart cells (Figure 2A). Based on polymer characterization data (Figure 1), PLT32i was selected to provide slowly surface-eroding vascular and muscle templates that were envisioned to help guide organized repair of damaged heart tissue, and PGS was chosen to provide a rapidly degrading vascular-parenchymal interface envisioned to accelerate transport and direct contact between vascular and parenchymal cells. The two primary pore architectures were: (i) vascular-like microchannels,[8b, 17] and (ii) rectangular grids.[13c, 16] The microchannels were ~2 cm long, ~100 μm high and ~100 μm wide separated by 30 μm wide ribs, while the rectangular grids had ~600 μm long, ~400 μm wide pores separated by 125 μm wide struts and were stacked with their short struts offset. Secondary pores, microtemplated using sintered spheres,[4b, 19] were generated within precisely fabricated molds, i.e., either silicon (Si) wafers etched with vascular-like microchannel patterns or polycarbonate (PC) molds hot-embossed with rectangular grid patterns.

PLT32i microchannels and grids were microtemplated in Si and PC molds containing sintered 5 to 20 μm spheres based on preliminary studies showing these spheres could be ready sintered in the confines of the molds. Porous PGS membranes were fabricated in PDMS gaskets containing 33 to 38 μm spheres because similar porous PGS membranes, when inserted between a heart cell compartment and a vascular compartment of a perfused microfluidic scaffold increased heart cell viability in comparison with a solid PGS membrane interface.[8b] Previously, 20 to 40 μm sphere size enabled optimal host vascular infiltration of implanted scaffolds, albeit constructed from materials other than those tested herein.[4b, 11a] Representative scanning electron micrographs of microporous components

(PLT32i microchannels, PGS interface, and PLT32i grids) and assembled scaffolds are provided in Figures 2B–D,F–G. The porosity of PLT32i microchannels with secondary pores is expected to be similar to porous PLT32i membranes (~58%, Figure 1D), while the porosity of PLT32i grids with primary rectangular through-pores and struts with secondary pores is estimated to be higher (~83%).

PLT32i grids with and without secondary pores were subjected to tensile mechanical testing in two orthogonal directions by applying strain in parallel to either the long or short side of the rectangular pores (Figure 2E).[13a] Mechanical compliance and anisotropy were demonstrated with respect to Young's modulus (E_{LONG}, 0.141 ± 0.029 MPa *versus* E_{SHORT}, 0.104 ± 0.022 MPa, $P<0.005$) and storage modulus at 1 Hz (E'_{LONG}, 0.204 ± 0.041MPa *versus* E'_{SHORT}, 0.142 ± 0.040 MPa, $P<0.005$). For comparison, Young's moduli for human myocardium were reportedly ~0.01 to 0.02 MPa at the start of diastole and 0.20 to 0.50 MPa at the end of diastole.[9b, 12] Future studies can investigate the mechanical properties of grids under conditions such as hydration and cell culture which are expected to lower scaffold stiffness.[13a, 25]

2.3. Vascular Cell Culture

To assess the behavior of cultured vascular cells, human umbilical vein endothelial cell (HUVEC) retention on fibronectin pre-treated PLT32i microchannel scaffolds was studied first over 5 days of static culture on open microchannels (Figure 3A–F) and subsequently for 5 days of perfusion culture in closed microchannels (Figure 3G–H). The first trials investigated cell seeding density and whether or not secondary pore presence increased vascular cell retention. Subsequent trials established conditions of perfusion culture that enabled vascular cell retention in closed microchannels with and without secondary micropores. The channel dimensions tested herein were within the size range of natural vasculature,[26] and were similar to those of perfusable PDMS-and-glass devices in which HUVECs attached to channels with square or circular cross sections,[27] with more stable attachment shown for the circular, more physiological channel geometry.[27b] The present study measured higher cell (DNA) content on culture day 2 than day 5 (Figure 3A–B), which may be due to an early loss of cells that were initially loosely adherent at the sharp corners of the square microchannels but were unable to form a stable attachment. On culture day 5, the endothelial cells were seen lining the flow channels and had utilized most of the available space under all conditions tested (Figure 3C–H). Co-staining with actin and CD-31, an endothelial cell marker,[28] demonstrated cell retention and cobblestone morphology on the open microchannels,[29] while a fluorescent cell-tracking dye demonstrated cell retention in the closed, perfused microchannels. While secondary micropores did not provide a clear benefit to the vascular cells in the device configuration tested herein, future device configurations are envisioned as stacked modular units comprising heart cell layers paired with dedicated, permeable microchannel layers,[8b] and in this envisioned configuration the secondary pores in the microchannels are expected to provide advantages of enabling transport between the individual modules and also reducing polymer volume fraction.

2.4. Heart Cell Alignment and Retention

Heart muscle scaffolds were tested to investigate the behaviors of cultured heart cells. The scaffolds comprised two PLT32i grids with rectangular through-pores that were stacked with the short struts offset and bonded to a porous PGS membrane according to a design shown to retain heart cells in vitro,[8b] and in vivo.[16] The scaffolds were seeded with a mixture of heart cells in fibrin gel, cultured statically for up to 5 days, and evaluated for cell number by DNA content and cell alignment using OrientationJ.[30] Heart cell retention was increased by the presence of secondary pores (Figure 4A), a finding that may be attributed to an increased surface area available for cell-scaffold interaction similar to a previous report.[31] Heart cell guidance according to the 3D path extending over and under the struts of the offset rectangular grids was demonstrated by confocal microscopy (Figure 4B–E) and was consistent with our previous report.[13c] Pixel-by-pixel image analysis was used to calculate coherency coefficients,[30b] which were similar for scaffolds with and without secondary pores (0.33 ± 0.01 and 0.28 ± 0.08, respectively), where a value of 0 or 1 denoted either random or uniform cell orientation. Circular histograms of cell orientation data showed cells that were predominantly aligned in parallel to the long axis of the rectangular pore, which was arbitrarily represented by the values of 0° and 180° in the graphs (Figure 4F,G).

2.5. Functionally Connected Heart Cells

The formation of functional connections between cultured heart cells was explored by calcium (Ca^{2+}) optical mapping using the same heart muscle scaffolds described in Section 2.4. On culture day 5, the engineered heart constructs were loaded with Fluo-4 AM, a fluorescent Ca^{2+} indicator dye,[32] to image, quantify and map spontaneous transient intracellular Ca^{2+} signaling.[33] Ca^{2+} transients, which are triggered by cardiac action potentials, play a major role in signal regulation within and between cardiomyocytes,[34] and provide a contractility index for cardiomyocytes cultured over different spatial scales.[33] Spontaneous Ca^{2+} transients were observed every 2 to 4 s and were quantified by normalizing the average signal intensity by the maximum and minimum fluorescence in selected regions of interest (ROIs) (Figure 5A–D). Time-activation maps were also created by simultaneously recording Ca^{2+} transients over the specimen surface for several hundred ms (Figure 5E–F). The findings of spontaneous and nearly simultaneous contraction of multiple neighboring heart cells suggest excitation-contraction coupling and functional connections between the cells. Future studies can be done to correlate optical indexes of contractility demonstrated here with direct contractile force measurements.[35]

2.6. Functional, Spatially Organized Co-cultures

Viable, spatially organized tissue was demonstrated after sequential seeding of the vascular template with HUVECs and the heart muscle scaffold with a heart cell-fibrin gel mixture followed by perfusion of culture medium through the microchannels for 5 days (Figure 6A–B). The HUVECs and heart cells, which were pre-labeled using fluorescent cell tracking dyes with two different emission spectra, were co-cultured using standard vascular cell medium shown to support both cell populations (Figure S1). The heart cells exhibited functional connectivity and synchronous contractility after 5 days of co-culture with perfusion (Figure 6C–E). Time-activation maps of the heart cells demonstrated Ca^{2+} signal

propagation over a distance of 2 to 3 mm, with spontaneous Ca^{2+} transients observed approximately every 2 s. Heart cells were present within the PLT32i grids and at the interface between the grids and porous PGS membrane, and vascular cells were present within the PLT32i microchannels, as seen in full cross-sectional images obtained after co-culture (Figure 6F) and microchannels visualized by removing the upper device layers after co-culture (Figure 6G). These findings demonstrate spatial organization and retention of co-cultured heart and vascular cells in the context of a perfusable multi-compartmental scaffold.

Current tissue engineering strategies include "pre-vascularization" wherein a scaffold is seeded with vascular cells and cultured in vitro with the objective of building a 3D structure with a rudimentary vascular network, with endothelial cells lining the inner surfaces of a 3D microvessel structure and a maximum distance between microvessels of approximately 200 μm.[5c] Although the current findings did not demonstrate specific effects of perfusion or HUVECs on the function of heart cells, a perfusion-mediated increase in myocyte viability was reported for a similar device wherein heart cells were separated from flow channels by a porous PGS membrane,[8b] and the simple presence of vascular cells is known to benefit cultured heart cells via paracrine signaling.[2a–c, 2e] For example, vascular endothelial cell growth factor (VEGF) produced by endothelial cells within implanted cardiac sheets enhanced the structural integration and function of cardiomyocytes.[2b] While previous studies of non-degradable materials demonstrated perfused endothelial cell-lined microchannels,[27] the present study, and recent reports,[8b, 17] extends the application space to biodegradable, implantable scaffolds. While the testing of scaffolds and cellularized devices in a cardiac implantation model was beyond the scope of the present work, future testing on the myocardium and in the setting of an infarction will be necessary, because differences in implantation site and local conditions are known to affect the degradation rate and performance of biomaterial implants.[36] In a cardiac implant model it will be important to determine whether PLT32i scaffolds can support infarct healing over its typical time course,[37] and to quantify host immune responses, cardiomyocyte survival and retention, and functional vascular integration.

3. Conclusion

In summary, a tissue engineering scaffold was built by combining two surface-eroding elastomers, one (PLT32i) newly designed to be photocurable and slowly biodegradable, and the other (PGS) already known to biodegrade rapidly. Polymer templates were fabricated, cellularized, assembled, and perfused to engineer contractile, pre-vascularized heart tissue. The PLT32i provided a hierarchical architecture of macroscale pore channels that enabled robust perfusion and guided heart cell alignment and microscale pores that increased heart cell retention while reducing polymer volume fraction, while the PGS served as a microporous vascular-parenchymal interface that provided high oxygen permeance.

4. Experimental Section

Polymer Synthesis

A UV cross-linking chamber (UVP CL-1000, 365 nm bulbs, 5 mW/cm^2) was positioned on top of a magnetic stir plate and used to synthesize PLT32i prepolymer in three steps. Step 1

reagents (1.0 molar equivalents limonene (f=2 C=C), 0.25 molar equivalents of TMPTMP (f = 3 –SH, Sigma), and 0.025 % (w w^{-1}) of 2,2-dimethoxy-2-phenylacetephenone (DMPA, Sigma) with respect to Step 1 constituents) were massed in 100 mL glass bottles with magnetic stir bars and irradiated for 3 h with stirring. Step 2 reagents (0.25 molar equivalents TMPTMP and 0.025 % (w w^{-1}) of DMPA with respect to Step 1 constituents) were then added to the reaction mixtures in the same glass bottles and irradiated for an additional 3 h with stirring. For Step 3, 0.575 molar equivalents of TEGBMP (f = 2–SH, Wako, Osaka, JA) with respect to Step 1 constituents and DMPA to afford an overall 1 % (w w^{-1}) concentration were added to the reaction mixture, which was heated to 80°C for 2 h to enable DMPA dissolution. The PLT32i prepolymer was stored in the dark at ambient temperature. The PLT32o pre-polymer was synthesized and cured as previously described,[16] according to methods identical to those describe above for PLT32i synthesis except that the co-monomer added in Step 3 was 1,10 DDT rather than TEGBMP. The PGS pre-polymer was synthesized as previously described,[10a] with minor modifications.[16] Briefly, 1.0 mol glycerol and 1.333 mol sebacic acid were reacted under N_2 at 140°C for 24 h, and after 24 h the PGS prepolymer was poured from the flask in which it was synthesized into a glass bottle to which 200 proof ethanol was added to afford a working solution of 33 % (w w^{-1}) prepolymer.

Polymer Degradation

Large, thick specimens of porous PLT32o, PLT32i, or PGS were utilized for polymer degradation studies to allow accurate monitoring of specimen dry mass as it decreased over time. Sintered acrylic sphere pore templates (disks that were 50 mm diameter x 15 mm thick, Healionics Inc., Seattle, WA) were divided into ~1 g wedge-shaped specimens (sides that were ~20 mm, ~17 mm, and ~15 mm). To enable complete infiltration and curing of the prepolymers within the templates, specimens were incubated with the prepolymer of interest at RT and 40 mTorr for 48 h, and then the PLT32o and PLT32i were UV irradiated for a duration of 16 h followed by post curing at 120°C and 40 mTorr for 24 h, whereas the PGS was cured at 120°C and 40 mTorr for 72 h.

The acrylic was leached out by serial immersion in dichloromethane, acetone, ethanol, and water. After lyophilization and recording of initial dry weight, each specimen was placed in a 50 mL conical tube containing 5 mL of either lipase (2300 U/mL, Sigma L0777) or PBS (GIBCO 10010023), and incubated at 37°C with slow orbital mixing. At timed intervals, each specimen was frozen, lyophilized, and its dry weight was recorded, after which it was returned to its conical tube and used for further study. The enzyme or PBS in the tubes was replaced twice per week.

Oxygen Permeance

Solid and porous polymer membranes were tested using a glass Franz cell apparatus fitted with fiber optic O_2 probes (OE-002, Lucid Scientific) on a magnetic stir plate. Small thin (≤ 1 mm thick) polymer specimens were needed for oxygen permeance to allow specimens to fit into the Franz cell. Consequently, PLT32o and PLT32i specimens were fabricated by a UV irradiation duration of 2 h followed by post-curing at 120°C and 40 mTorr for 24 h, whereas PGS specimens were cured at 120°C and 40 mTorr for 72 h.[16] A test specimen

was sealed between the two chambers (donor, acceptor) of the Franz cell, a stir bar was placed in the acceptor chamber, and the device was filled with water. The donor chamber was sparged with N_2 until it had equilibrated to zero percent O_2, then the donor chamber was sparged with room air and the partial pressure of O_2 in each chamber was recorded over time. Permeance (cm^3 S.T.P. cm^{-2} s^{-1} $cmHg^{-1}$) was calculated in the linear region of the resulting curve (R^2>0.96).[22, 38]

Vascular-Parenchymal Interface

PGS interfaces with secondary pores were fabricated using a PDMS-on-glass mold and PMMA spheres with an average (range) diameter of 35 μm (33 – 38 μm) (PMPMS, Cospheric, Santa Barbara, CA). A mixture of PMMA spheres in 200 proof ethanol (~300 mg/mL) was dispensed into a 4 cm × 4 cm PDMS gasket sealed to a flat glass surface and, after ethanol evaporation and gasket removal, sintered together in a 120°C oven for 24 h. PGS prepolymer (33 % (w w^{-1}) in ethanol) was added to the mold, and after ethanol evaporation, cured at 120°C and 40 mTorr for 72 h. The specimens were then immersed in acetone for 18 h (to remove unreacted sol and PMMA), an excess of 200 proof ethanol for 24 h (to ensure sol removal), and washed in water.

Grids

PLT32i grids with secondary pores were fabricated using PC molds hot-embossed to produce grids with rectangular through-pores,[16] and PMMA spheres with an average (range) diameter of 12 μm (5 – 20 μm) (Cospheric). A mixture of PMMA spheres in ethanol (~300 mg/mL) was added to the mold, and after ethanol evaporation, sintered together in a 120°C oven for 24 h. PLT32i prepolymer was dispensed onto the sintered spheres within the mold, UV irradiated for 2 h, established to be a sufficient duration for the ~100 μm thick grids, and post-cured at 120°C and 40 mTorr for 24 h. Other grids without secondary pores were cast and cured in PC molds without PMMA spheres. The specimens were then immersed for 10 min in 1,4 dioxane (to de-mold by dissolving the surface of the PC), acetone for 24 h (to remove unreacted sol and, if present, PMMA), ethanol, and water.

To assess mechanical properties and anisotropy, grids with secondary pores were cut into strips that were oriented either in parallel or orthogonal to the long axis of the through-pores.[13a] Specimen thickness was measured using a Starrett dial indicator, and gauge length and width were measured using calipers after specimens were mounted in a DMA Q800 (TA Instruments, New Castle, DE). Specimens were strained to failure in the Multi-Frequency/Strain mode under a controlled force setting with a preload force of 0.001N and a ramp force from 0.05 N/min to 0.5 N/min.[16] Young's moduli were determined by linear regression of the stress strain curve over a strain range of 0.005 to 0.10 mm mm^{-1} (R^2>0.98). The UTS was taken as the maximum stress measured prior to the onset of failure.

Microchannels

PLT32i microfluidic base parts with secondary pores were fabricated using Si wafer molds etched to produce microchannels,[8b, 17] and PMMA spheres with an average (range) diameter of 12 μm (5 – 20 μm) (Cospheric). After mold cleaning in piranha solution and spin-coating with a sacrificial layer of maltose,[17] the 2 cm × 2 cm central area was

bounded by a PDMS gasket. Approximately 100 mg of PMMA spheres were dispensed dry into the microchannels of the mold and sintered together a 120°C oven for 24 h. PLT32i prepolymer was added into the mold onto the sintered spheres and also the inlet and outlet transitional zones after the entire etched area was bounded by a large PDMS gasket. The PLT32i microchannels were UV irradiated for 2 h, established to be a sufficient duration for the <300 μm thick components, post-cured at 120°C and 40 mTorr for 24 h, immersed in 60°C water for 2 days (to de-mold and dissolve the maltose), acetone for 24 h (to remove the PMMA), ethanol, and water.

Cell Culture Studies

HUVECs (PCS-100-010, American Type Culture Collection (ATCC), Manassas, VA, passage 3–5) were expanded and cultured in vascular cell medium (i.e., Basal Medium (ATCC PCS100-300) supplemented with Endothelial Cell Growth Kit (ATCC PCS100-040) and 1% penicillin/streptomycin (P/S)). Scaffolds for initial cultures on open microchannels were 6 mm diameter PLT32i disks. The scaffolds were autoclave-sterilized, pre-treated with fibronectin (20 μg/mL at 37°C for 24 h), and placed within PDMS gaskets within 24-well plates. HUVECs were seeded on scaffolds at either a low (0.64 million cells cm^{-2}) or high (2.5 million cells cm^{-2}) initial cell density using an initial volume of 30 μL per disk. After 30 min, an additional 2 mL of media were added to the wells; media were completely replaced every 2 days. For subsequent studies of closed microchannels, the scaffolds were PLT32i microfluidic base parts with optically transparent covers, inlet and outlet transition zones, and tubing to enable perfusion.[8b, 17] HUVECs were pre-labelled by incubation in CellTracker (25 μM in culture medium, Thermo C12881) and injected into the microchannels via the inlet port. After 3 h of incubation under static culture conditions, perfusion was established at a rate of 3 μL/min for the first 24 h and then at 10 μL/min for the remainder of the 5 day culture.

Heart cells were isolated from 1–2 day old neonatal rats as previously described,[13c] according to an Institutional Animal Care and Use Committee (IACUC) approved protocol, and cultured in Dulbecco's Modified Eagle's Medium (DMEM) supplemented with 10% horse serum, 2% fetal bovine serum, and 1% P/S. Scaffolds for initial cultures were 6 mm diameter disks comprising porous PGS membranes combined with two offset PLT32i grids that were cured at 120°C and 40 mTorr for 18 h.[16] The scaffolds were sterilized, pre-treated with fibronectin and placed into PDMS gaskets within 24-well plates as described above for HUVECs. A mixture of heart cells (3 to 4 million cells cm^{-2}) in 3.3 mg/mL fibrin gel were seeded on scaffolds using an initial volume of 30 μL per disk. After the fibrin gel was allowed to solidify for ~30 min, an additional 2 mL of media were added to the wells; media were completely replaced every 2 days.

For subsequent studies of scalable units, two scaffold components were pre-fabricated: (i) a heart cell scaffold comprising a 2 cm × 2 cm PGS porous interface bonded to two short strut offset PLT32i grids (1.6 cm diameter) and (ii) a PLT32i microfluidic base part that was closed by an optically transparent cover with a 2 cm × 2 cm square cut-out positioned over the central microchannels and surrounded by PDMS walls to provide a culture medium reservoir, inlet and outlet transition zones, and tubing to enable perfusion (Figure 6A,B).

First, HUVECs that were pre-labeled with CellTracker Blue were dispensed through the central opening and onto fibronectin-pre-treated microchannels at an initial cell density of 2.5 million cells cm^{-2} and cultured statically for 24 h. Second, the heart cell scaffold was placed onto the endothelialized microchannels and attached using fibrin gel (3.3 mg/mL, 100 μL). Third, heart cells that were pre-labeled with CellTracker Red were mixed in fibrin gel and dispensed onto the heart cell scaffold at an initial cell density of ~3.5 million cells cm^{-2} and cultured statically for 1 h. Fourth, vascular cell culture medium was added to the reservoir, the microfluidics were connected to the flow circuit,[8b, 17] and perfusion was established at a rate of 10 μL/min. The co-culture was carried out for 5 days under conditions of continuous perfusion and the medium in the reservoir was exchanged every 2 days.

DNA Assay

DNA was quantified following enzymatic digestion of specimens in buffered 0.125 mg/mL papainase solution for 16 h at 60°C. The number of cells per specimen was assessed by the PicoGreen dsDNA assay,[13a] assuming mononuclear HUVECs and neonatal rat heart cells, and 7.6 pg of DNA per cell.[39]

Calcium Ion Imaging

For Ca^{+2} imaging studies, scaffolds with cultured heart cells were incubated in Fluo4-AM dye as previously described.[32] Briefly, constructs were incubated for 20 min in a solution of 10 μL/mL of Fluo-4 AM (ThermoFisher F-14217) in DMEM and then for another 20 min in Tyrode's solution. Imaging was performed in a 37°C, 5% CO_2/95% room air environment using a Zeiss AxioObserver epifluorescence inverted microscope with a high speed Hamamatsu ORCA Flash 4.0 sCMOS camera. The acquired images were processed using Zen Software (Carl Zeiss Inc., Black Edition) to determine the mean, maximum, and minimum intensities for each frame within selected regions of interest (ROI). MATLAB was then used to plot the relative fluorescence intensities over time by normalizing the average intensity by the maximum and minimum intensities in the region of interest. The images were also processed in MATLAB by smoothing the images both spatially and temporally, removing the background pixel intensity, and using a threshold value for excitation to create an activation heat map.[40]

Immunohistochemical Analyses

Endpoint specimens of scaffolds with cultured cells were fixed in 10% neutral buffered formalin, permeabilized using 0.2% Triton X-100, blocked with 1% bovine serum albumin, and imaged on a Zeiss LSM700 confocal microscope. Specimens were stained with phalloidin-Alexa Fluor 488 (ThermoFisher A12379) to visualize filamentous actin and, in some cases, co-stained with CD-31 (R&D Systems BBA7) and secondary antibody (R&D Systems HAF018) to help identify endothelial cells. The actin fiber alignment analysis was performed using OrientationJ, an ImageJ plug-in.[30a] Briefly, a Gaussian distribution weighting function with a standard deviation of one pixel specified an area of interest around each pixel within each image, Cubic-B spline interpolation was used to compute the partial spatial derivatives in the x and y directions and assign a structure tensor to each pixel, and these data were used to obtain the local orientation and coherency for each pixel. A

coherency coefficient was calculated as an index of local fiber alignment, where a value close to one indicates coherent fiber orientation in one direction, while a value close to zero represents no dominant fiber orientation.

Statistical Analysis

Data were analyzed by analysis of variance (ANOVA) using Prism (GraphPad Software, Inc. La Jolla, CA). Individual differences between groups were determined by Turkey's *post hoc* analysis and statistical significance was established at $P<0.05$.

Supplementary Material

Refer to Web version on PubMed Central for supplementary material.

Acknowledgments

This work was funded by NIH/NHLBI Grant R01-HL107503 (to LEF). The authors are grateful to E.S. Kim for his help with drawings and T. Quach for her help with the degradation studies.

References

1. Mozaffarian D, Benjamin EJ, Go AS, Arnett DK, Blaha MJ, Cushman M, de Ferranti S, Despres JP, Fullerton HJ, Howard VJ, Huffman MD, Judd SE, Kissela BM, Lackland DT, Lichtman JH, Lisabeth LD, Liu S, Mackey RH, Matchar DB, McGuire DK, Mohler ER 3rd, Moy CS, Muntner P, Mussolino ME, Nasir K, Neumar RW, Nichol G, Palaniappan L, Pandey DK, Reeves MJ, Rodriguez CJ, Sorlie PD, Stein J, Towfighi A, Turan TN, Virani SS, Willey JZ, Woo D, Yeh RW, Turner MB. Circulation. 2015; 131:e29. [PubMed: 25520374]
2. a) Stevens KR, Kreutziger KL, Dupras SK, Korte FS, Regnier M, Muskheli V, Nourse MB, Bendixen K, Reinecke H, Murry CE. Proc Natl Acad Sci U S A. 2009; 106:16568. [PubMed: 19805339] b) Masumoto H, Matsuo T, Yamamizu K, Uosaki H, Narazaki G, Katayama S, Marui A, Shimizu T, Ikeda T, Okano T, Sakata R, Yamashita JK. Stem Cells. 2012; 30:1196. [PubMed: 22438013] c) Ye L, Zimmermann WH, Garry DJ, Zhang J. Circ Res. 2013; 113:922. [PubMed: 24030022] d) Sekine H, Shimizu T, Sakaguchi K, Dobashi I, Wada M, Yamato M, Kobayashi E, Umezu M, Okano T. Nat Commun. 2013; 4:1399. [PubMed: 23360990] e) Ye L, Chang YH, Xiong Q, Zhang P, Zhang L, Somasundaram P, Lepley M, Swingen C, Su L, Wendel JS, Guo J, Jang A, Rosenbush D, Greder L, Dutton JR, Zhang J, Kamp TJ, Kaufman DS, Ge Y. Cell Stem Cell. 2014; 15:750. [PubMed: 25479750] f) Chong JJ, Yang X, Don CW, Minami E, Liu YW, Weyers JJ, Mahoney WM, Van Biber B, Cook SM, Palpant NJ, Gantz JA, Fugate JA, Muskheli V, Gough GM, Vogel KW, Astley CA, Hotchkiss CE, Baldessari A, Pabon L, Reinecke H, Gill EA, Nelson V, Kiem HP, Laflamme MA, Murry CE. Nature. 2014; 510:273. [PubMed: 24776797] g) Komae H, Sekine H, Dobashi I, Matsuura K, Ono M, Okano T, Shimizu T. J Tissue Eng Regen Med. 2015; doi: 10.1002/term.1995
3. a) Baranski JD, Chaturvedi RR, Stevens KR, Eyckmans J, Carvalho B, Solorzano RD, Yang MT, Miller JS, Bhatia SN, Chen CS. Proc Natl Acad Sci U S A. 2013; 110:7586. [PubMed: 23610423] b) Moya ML, Hsu YH, Lee AP, Hughes CC, George SC. Tissue Eng, Part C. 2013; 19:730.c) Chaturvedi RR, Stevens KR, Solorzano RD, Schwartz RE, Eyckmans J, Baranski JD, Stapleton SC, Bhatia SN, Chen CS. Tissue Eng, Part C. 2015; 21:509.
4. a) Freed LE, Engelmayr GC Jr, Borenstein JT, Moutos FT, Guilak F. Adv Mater. 2009; 21:3410. [PubMed: 20882506] b) Madden LR, Mortisen DJ, Sussman EM, Dupras SK, Fugate JA, Cuy JL, Hauch KD, Laflamme MA, Murry CE, Ratner BD. Proc Natl Acad Sci U S A. 2010; 107:15211. [PubMed: 20696917]
5. a) Cassell OC, Hofer SO, Morrison WA, Knight KR. Br J Plast Surg. 2002; 55:603. [PubMed: 12550111] b) Radisic M, Deen W, Langer R, Vunjak-Novakovic G. Am J Physiol: Heart Circ

Physiol. 2005; 288:H1278. [PubMed: 15539422] c) Novosel EC, Kleinhans C, Kluger PJ. Adv Drug Delivery Rev. 2011; 63:300.d) Sun X, Altalhi W, Nunes SS. Adv Drug Delivery Rev. 2016; 96:183.

6. a) Gratson GM, Xu M, Lewis JA. Nature. 2004; 428:386. [PubMed: 15042080] b) Melchels FP, Domingos MA, Klein TJ, Malda J, Bartolo PJ, Hutmacher DW. Prog Polym Sci. 2012; 37:1079.c) Tumbleston JR, Shirvanyants D, Ermoshkin N, Janusziewicz R, Johnson AR, Kelly D, Chen K, Pinschmidt R, Rolland JP, Ermoshkin A, Samulski ET, DeSimone JM. Science. 2015; 347:1349. [PubMed: 25780246]
7. a) Hanson Shepherd JN, Parker ST, Shepherd RF, Gillette MU, Lewis JA, Nuzzo RG. Adv Funct Mater. 2011; 21:47. [PubMed: 21709750] b) Miller JS, Stevens KR, Yang MT, Baker BM, Nguyen DH, Cohen DM, Toro E, Chen AA, Galie PA, Yu X, Chaturvedi R, Bhatia SN, Chen CS. Nat Mater. 2012; 11:768. [PubMed: 22751181] c) Gurkan UA, Fan Y, Xu F, Erkmen B, Urkac ES, Parlakgul G, Bernstein J, Xing W, Boyden ES, Demirci U. Adv Mater. 2013; 25:1192. [PubMed: 23192949] d) Kolesky DB, Truby RL, Gladman AS, Busbee TA, Homan KA, Lewis JA. Adv Mater. 2014; 26:3124. [PubMed: 24550124] e) Pati F, Jang J, Ha DH, Won Kim S, Rhie JW, Shim JH, Kim DH, Cho DW. Nat Commun. 2014; 5:3935. [PubMed: 24887553]
8. a) Maidhof R, Marsano A, Lee EJ, Vunjak-Novakovic G. Biotechnol Prog. 2010; 26:565. [PubMed: 20052737] b) Ye X, Lu L, Kolewe ME, Hearon K, Fischer KM, Coppeta J, Freed LE. Adv Mater. 2014; 26:7202. [PubMed: 25238047]
9. a) Rai R, Tallawi M, Grigore A, Boccaccini AR. Prog Polym Sci. 2012; 37:1051.b) Chen Q, Liang S, Thouas GA. Prog Polym Sci. 2013; 38:584.
10. a) Wang Y, Ameer GA, Sheppard BJ, Langer R. Nat Biotechnol. 2002; 20:602. [PubMed: 12042865] b) Wu W, Allen RA, Wang Y. Nat Med. 2012; 18:1148. [PubMed: 22729285]
11. a) Thomson KS, Korte FS, Giachelli CM, Ratner BD, Regnier M, Scatena M. Tissue Eng, Part A. 2013; 19:967. [PubMed: 23317311] b) Stoppel W, Ghezzi C, McNamara S, LB, Kaplan D. Ann Biomed Eng. 2015; 43:657. [PubMed: 25537688]
12. Huyer LD, Montgomery M, Zhao Y, Xiao Y, Conant G, Korolj A, Radisic M. Biomed Mater (Bristol, U K). 2015; 10
13. a) Engelmayr GC Jr, Cheng M, Bettinger CJ, Borenstein JT, Langer R, Freed LE. Nat Mater. 2008; 7:1003. [PubMed: 18978786] b) Neal RA, Jean A, Park H, Wu PB, Hsiao J, Engelmayr GC Jr, Langer R, Freed LE. Tissue Eng, Part A. 2013; 19:793. [PubMed: 23190320] c) Kolewe ME, Park H, Gray C, Ye X, Langer R, Freed LE. Adv Mater. 2013; 25:4459. [PubMed: 23765688] d) Park H, Larson BL, Kolewe ME, Vunjak-Novakovic G, Freed LE. Exp Cell Res. 2014; 321:297. [PubMed: 24240126]
14. Park H, Larson BL, Guillemette MD, Jain SR, Hua C, Engelmayr GC Jr, Freed LE. Biomaterials. 2011; 32:1856. [PubMed: 21144580]
15. Guillemette MD, Park H, Hsiao J, Jain SR, Larson BL, Langer R, Freed LE. Macromol Biosci. 2010; 10:1330. [PubMed: 20718054]
16. Fischer KM, Morgan KY, Hearon K, Sklaviadis D, Tochka ZL, Fenton OS, Anderson DG, Langer R, Freed LE. Adv Healthcare Mater. 2016; 5:813.
17. Ye X, Lu L, Kolewe ME, Park H, Larson BL, Kim ES, Freed LE. Biomaterials. 2013; 34:10007. [PubMed: 24079890]
18. Pomerantseva I, Krebs N, Hart A, Neville CM, Huang AY, Sundback CA. J Biomed Mater Res, Part A. 2009; 91:1038.
19. Marshall A, Ratner B. AIChE J. 2005; 51:1221.
20. Lyu S, Untereker D. Int J Mol Sci. 2009; 10:4033. [PubMed: 19865531]
21. Hirt MN, Hansen A, Eschenhagen T. Circ Res. 2014; 114:354. [PubMed: 24436431]
22. a) Ismail, AF.; Matsuura, T.; Khulbe, K. Gas Separation Membranes. Springer; 2015. b) Hwang ST, Tang T, Kammermeyer K. J Macromol Sci, Part B: Phys. 1971; 5:1.
23. Yasuda H. J Polym Sci A1. 1967; 5:2952.
24. a) Gao J, Crapo PM, Wang Y. Tissue Eng. 2006; 12:917. [PubMed: 16674303] b) Li Z, Zou H, Liu P. RSC Adv. 2015; 5:37837.
25. Ifkovits JL, Devlin JJ, Eng G, Martens TP, Vunjak-Novakovic G, Burdick JA. ACS Appl Mater Interfaces. 2009; 1:1878. [PubMed: 20160937]
26. Folkman J, Hochberg M. J Exp Med. 1973; 138:745. [PubMed: 4744009]

27. a) Chau LT, Rolfe BE, Cooper-White JJ. Biomicrofluidics. 2011; 5:34115. [PubMed: 22662042] b) Zhang B, Peticone C, Murthy SK, Radisic M. Biomicrofluidics. 2013; 7:44125. [PubMed: 24404058]
28. Pusztaszeri MP, Seelentag W, Bosman FT. J Histochem Cytochem. 2006; 54:385. [PubMed: 16234507]
29. Jimenez N, Krouwer VJ, Post JA. Cytotechnology. 2013; 65:1. [PubMed: 22573289]
30. a) Fonck E, Feigl GG, Fasel J, Sage D, Unser M, Rüfenacht DA, Stergiopulos N. Stroke. 2009; 40:2552. [PubMed: 19478233] b) Duclos G, Garcia S, Yevick HG, Silberzan P. Soft Matter. 2014; 10:2346. [PubMed: 24623001]
31. O'Brien FJ, Harley BA, Yannas IV, Gibson LJ. Biomaterials. 2005; 26:433. [PubMed: 15275817]
32. Guatimosim S, Guatimosim C, Song LS. Methods Mol Biol. 2011; 689:205. [PubMed: 21153794]
33. Huebsch N, Loskill P, Mandegar M, Marks N, Sheehan A, Ma Z, Mathur A, Nguyen T, Yoo J, Judge L. Tissue Eng, Part C. 2015; 21:467.
34. a) Gergs U, Kirchhefer U, Buskase J, Kiele-Dunsche K, Buchwalow IB, Jones LR, Schmitz W, Traub O, Neumann J. J Mol Cell Cardiol. 2011; 51:682. [PubMed: 21871897] b) Fearnley CJ, Roderick HL, Bootman MD. Cold Spring Harbor Perspect Biol. 2011; 3:a004242.c) Li C, Meng Q, Yu X, Jing X, Xu P, Luo D. PLoS One. 2012; 7:361.
35. Bian W, Juhas M, Pfeiler TW, Bursac N. Tissue Eng, Part A. 2012; 18:957. [PubMed: 22115339]
36. a) Artzi N, Oliva N, Puron C, Shitreet S, Artzi S, Bon Ramos A, Groothuis A, Sahagian G, Edelman ER. Nat Mater. 2011; 10:704. [PubMed: 21857678] b) Oliva N, Unterman S, Zhang Y, Conde J, Song HS, Artzi N. Adv Healthcare Mater. 2015; 4:1584.
37. Holmes JW, Borg TK, Covell JW. Annu Rev Biomed Eng. 2005; 7:223. [PubMed: 16004571]
38. Yasuda H, Lamaze C. J Appl Polym Sci. 1972; 16:595.
39. Alsberg E, Anderson KW, Albeiruti A, Rowley JA, Mooney DJ. Proc Natl Acad Sci U S A. 2002; 99:12025. [PubMed: 12218178]
40. Laughner JI, Ng FS, Sulkin MS, Arthur RM, Efimov IR. Am J Physiol: Heart Circ Physiol. 2012; 303:H753. [PubMed: 22821993]

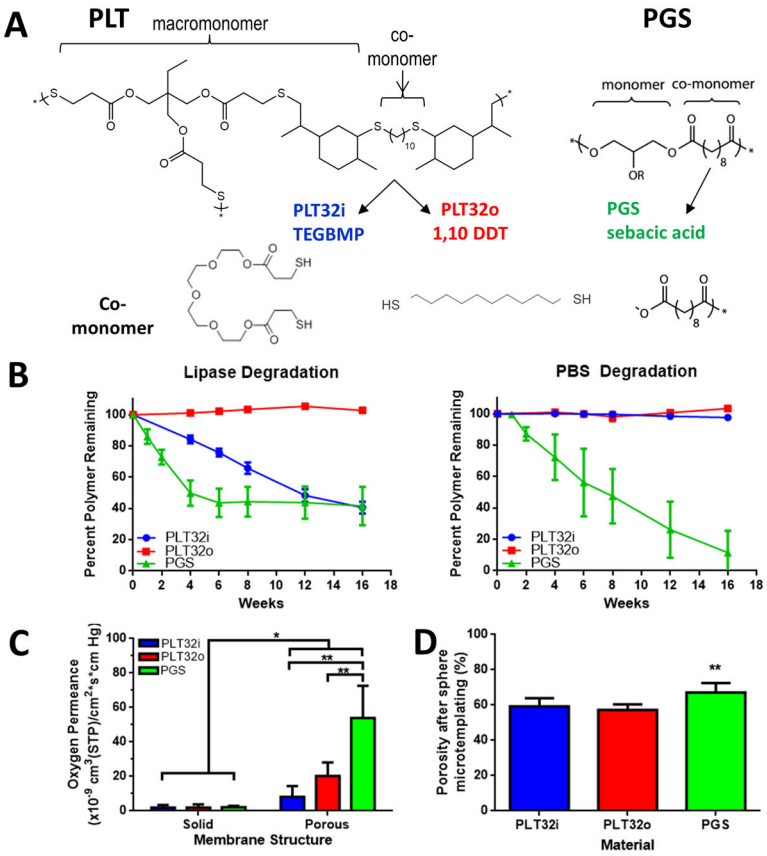

Figure 1. Multi-material approach

(A) Chemical formulations of PLT32i, based on D-Limonene, TMPTMP and TEGBMP, PLT32o,[16] and PGS,[10a]; (B) Degradation kinetics of the three materials in lipase or phosphate buffered saline (PBS); (C) Oxygen permeance for solid or porous membranes made of the three materials; (D) Porosity of microtemplated materials. Data are the average +/− SD of (B) n=4, (C) n=3 to 8, or (D) n=12 samples. *Significant effect of porosity, **Significant effect of material.

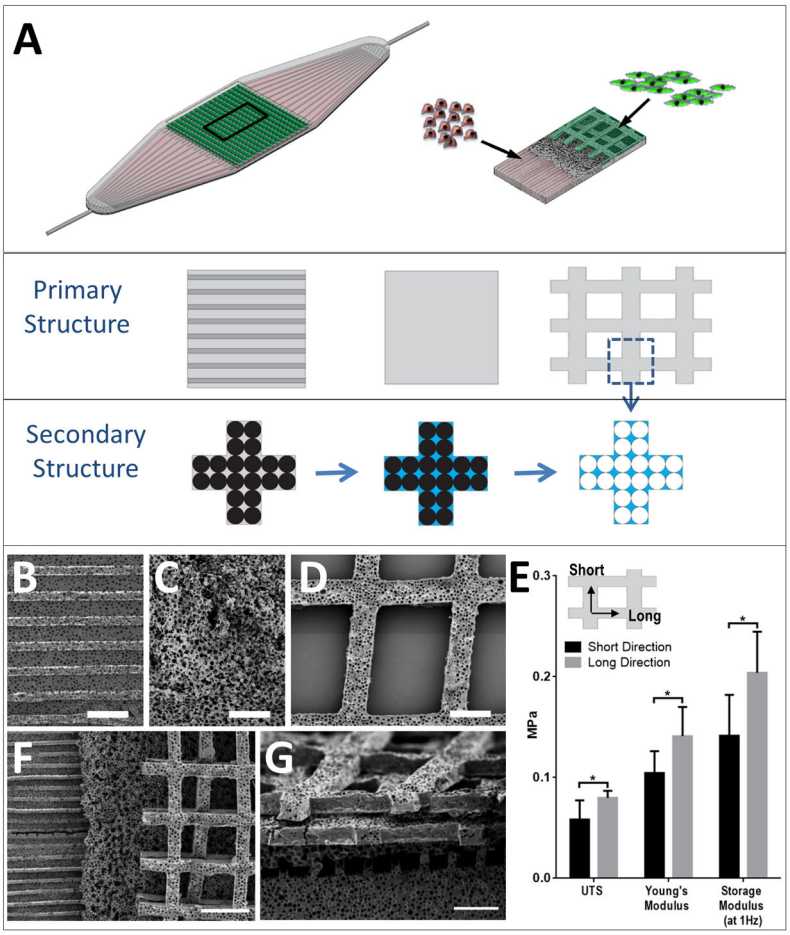

Figure 2. Hierarchical architecture

(A) Scaffolds for co-culturing vascularized cardiac tissue consist of perfusable channels for HUVECs (red), a vascular-parenchymal interface, and two offset grids with rectangular through-pores for heart cells (green). Primary and secondary pore structures were fabricated in the polymers by combining micromolding with porogen templating; (B–D, F–G) SEM images of: (B) porous channels; (C) porous interface; (D) porous grids; (F–G) assembled scaffold shown in two views. (B–D) Scale bars: (B–D, G) 200 μm; (F) 500 μm. (E) Mechanical properties (ultimate tensile strength (UTS), Young's modulus, and Storage Modulus at 1Hz) of grids tested by applying strain parallel to either the short or long side of the rectangular pores. *Significant anisotropy.

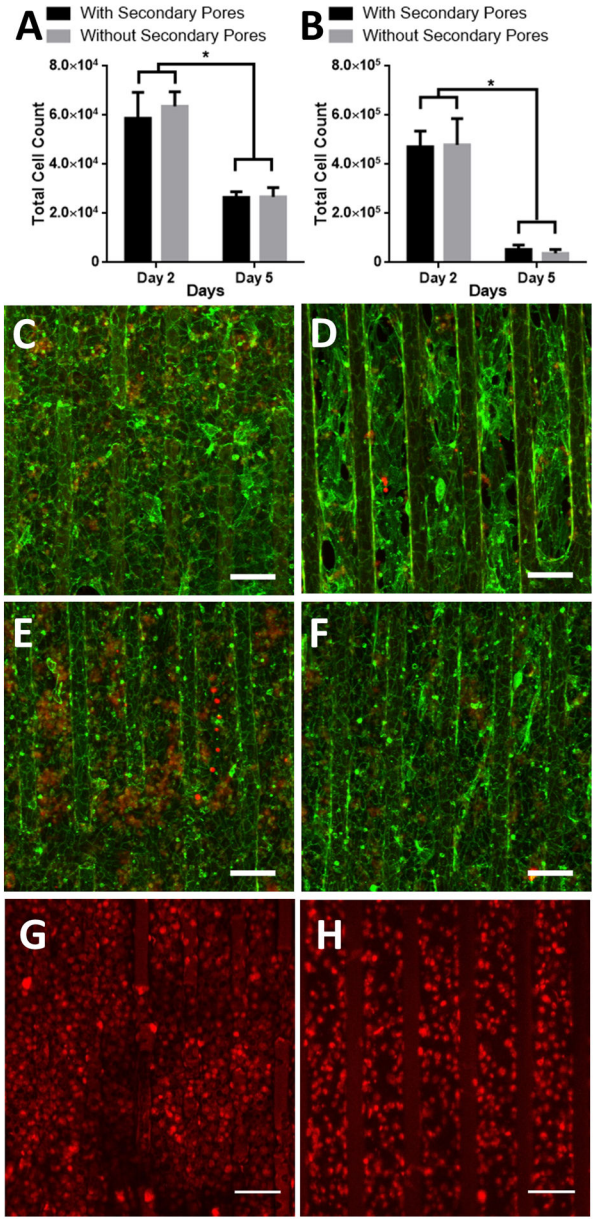

Figure 3. Vascular cell retention

HUVECs were cultured for five days on PLT32i scaffolds (A–F) statically on open microchannels and (G–H) with perfusion in closed microchannels. Initial cell seeding density was either (A) low or (B–H) high. Microchannels were fabricated either (C,E,G) with or (D,F,H) without secondary pores. (A,B) Number of cells per specimen; (C–H) Confocal microscopy images of cells on culture day 5. Stain: (C–F) actin (green) and CD-31 (red); (G,H) Cell Tracker (red). Scale bars 100 μm. Data are the average +/− SD of 6 samples. *Significant main effect of culture time.

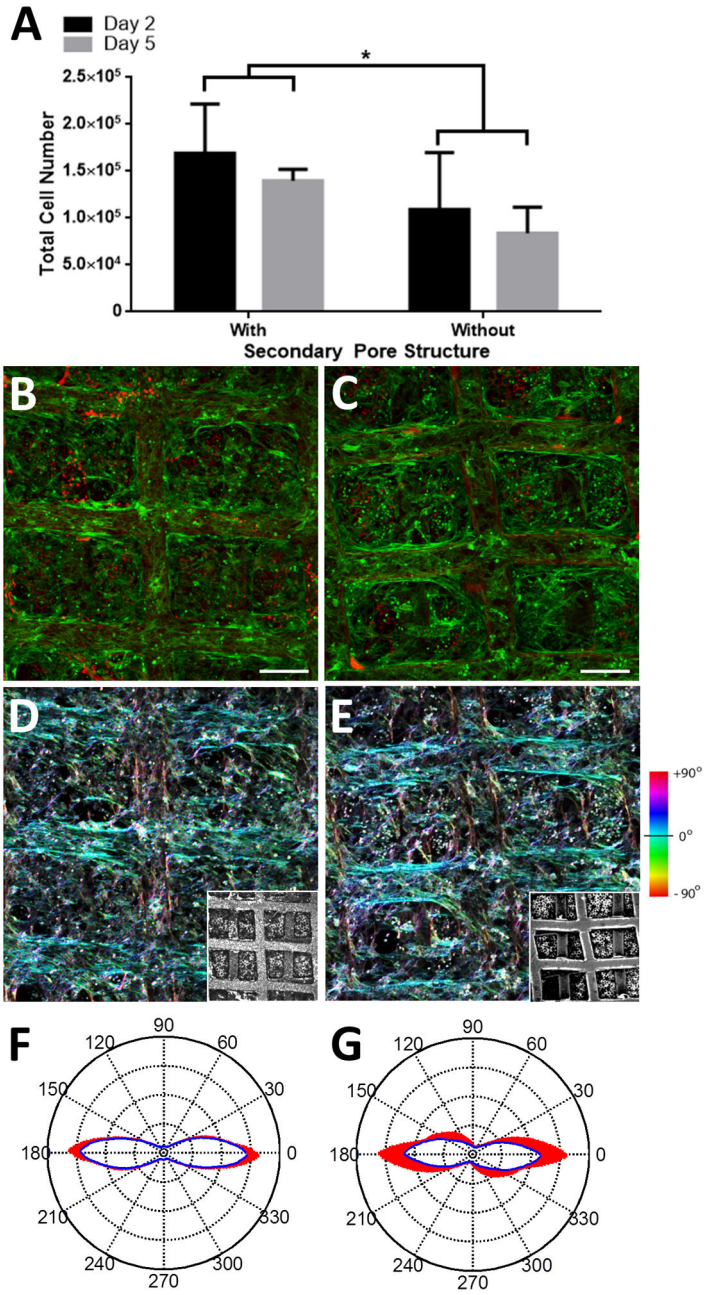

Figure 4. Heart cell retention and alignment

Heart cells were cultured for five days on porous PGS membranes combined with PLT32i grids either (B,D,F) with or (C,E,G) without secondary pores. (A) Number of cells per specimen; (B–E) Heart cell orientation on day 5 shown in confocal micrographs (B,C) before and (D,E) after pixel-by-pixel image analysis;[30] (F,G) Graphical representation of cellular alignment, showing a predominant alignment direction along the x- axis line (0° and 180°) and in parallel to the long axes of the rectangular pores. Co-stain: actin (green) and Draq5 (red, scaffold autofluorescence). Scale bars 100 μm. Data are the average +/− SD of 4

specimens for cell number and 2 fields of view for 3 or 4 specimens for cell orientation.
*Significant main effect of secondary pores.

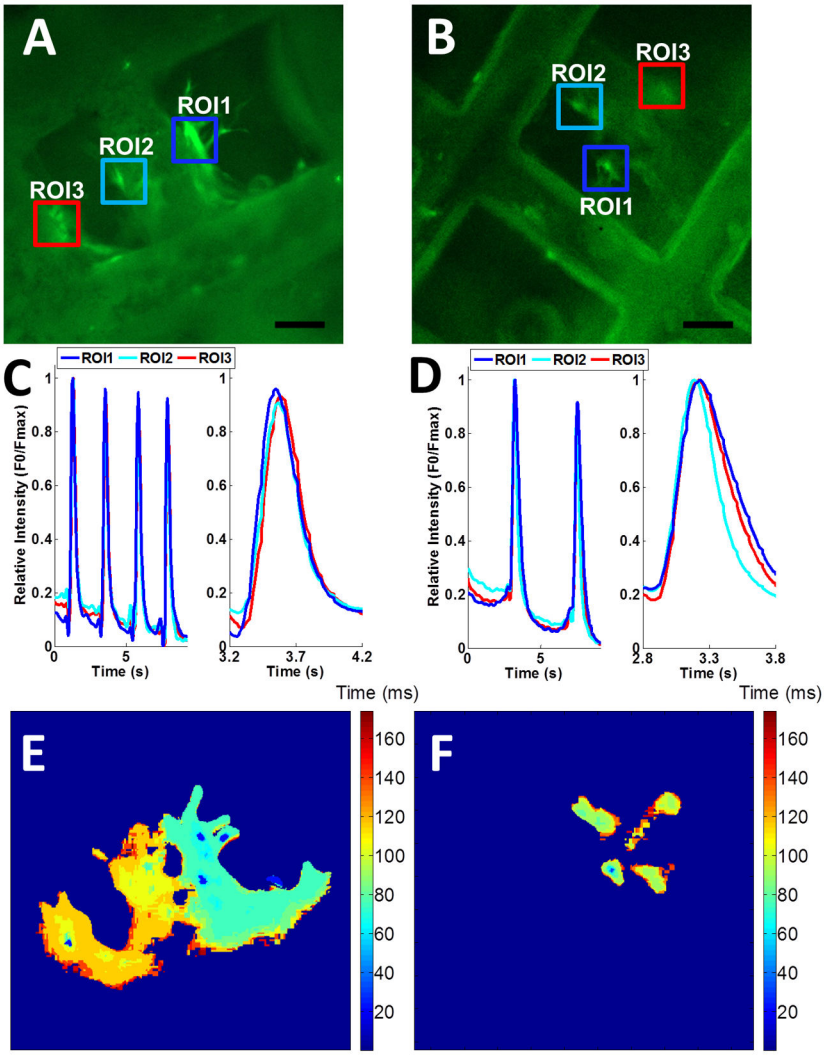

Figure 5. Functional connectivity of heart cells

Calcium imaging data for heart cells cultured for 5 days on porous PGS membranes combined with short strut offset PLT32i grids either (A,C,E) with or (B,D,F) without secondary pores. (A,B) Constructs stained with Fluo-4AM; (C,D) Intensity of Ca^{+2} signal over time in the selected ROIs. (E,F) Time activation maps showing excitation. Scale bars 100 μm. Data are from representative samples.

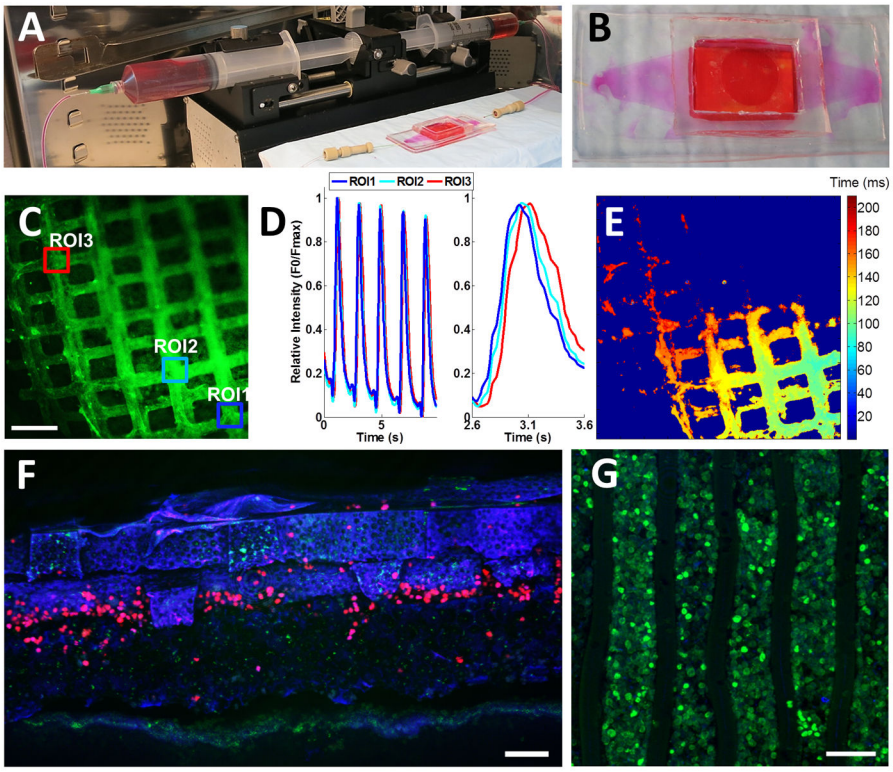

Figure 6. Functional, spatially organized co-cultures

Multi-compartmental scaffolds comprising two offset PLT32i grids with primary and secondary pores, a porous PGS interface, and porous PLT32i microchannels were seeded, with HUVECs in the channels and heart cells on the grids, and cultured with microchannel perfusion for 5 days. (A,B) Experimental set-up; (C–E) Ca^{+2} ion imaging of the heart cells (C) Construct stained with Fluo-4AM; (D) Intensity of Ca^{+2} signal over time in the selected ROIs. (E) Time activation maps showing excitation. (F,G) Spatial organization of heart and vascular cells in (F) a full cross-sectional view after co-culture (tracked heart and vascular cells respectively appear red and green) and (G) microchannels visualized by removing upper device layers after co-culture (actin-stained HUVECs appear green). Scale bars: (C) 500 μm, (F,G) 100 μm. Data are from representative samples.